Three-dimensional optical tomographic imaging of scattering objects in tissue-simulating turbid media using independent component analysis

M. Alrubaiee, M. Xu, S. K. Gayen, M. Brito, and R. R. Alfano[a)]
Institute for Ultrafast Spectroscopy and Lasers, Physics Department, The City College of New York and the Graduate School of the City University of New York, 138th Street at Convent Avenue, New York, New York 10031

(Received 6 April 2005; accepted 14 September 2005; published online 4 November 2005)

An information-theory-based approach for the detection and three-dimensional localization of scattering targets embedded in a turbid medium, such as a tumor in the breast, is introduced. The approach uses multisource illumination of the medium, multidetector transillumination signal acquisition, and independent component analysis of the information theory for target detection and localization. The efficacy of the approach is demonstrated by detecting and obtaining location information about scattering targets embedded in human breast tissue-simulating turbid media of thickness 50 times the transport mean-free path. © *2005 American Institute of Physics*.
[DOI: 10.1063/1.2130547]

Detection and localization of scattering targets within a turbid medium is a challenging problem with diverse practical applications, such as imaging of a breast tumor, identification of mines in coastal water, and detection of an airplane, or, structures through cloud and fog cover. A recent study involving 35 319 patients underscores the influence of primary tumor location on breast cancer prognosis, and makes it imperative that breast cancer detection modalities obtain three dimensional (3D) location of the tumor relative to the axilla.[1] Optical detection of targets in a turbid medium makes use of the difference in optical properties, such as scattering coefficient, absorption coefficient, index of refraction, and fluorescence between the targets of interest and the intervening medium.[2] Multiple scattering of light by the turbid medium produces a noise background that deteriorates the contrast, blurs the image, and in severe cases makes direct transillumination imaging impossible. Inverse image reconstruction approaches that are commonly used to retrieve image information have to deal with the fact that inverse problems are ill posed, and attain different measures of success with ~1 cm spatial resolution.[3]

This article introduces an alternative approach for detection and 3D localization of targets (optical inhomogeneities) embedded inside a highly scattering turbid medium. The approach makes use of transmitted light signal collected by multiple detectors following multiple-source illumination of the turbid medium containing the targets. The resulting multiple angular views provide robust data that is analyzed using the independent component analysis (ICA) (Ref. 4) of information theory to determine the locations of targets relative to the medium boundaries with millimeter accuracy. We refer to this optical domain application of ICA as OPTICA to distinguish it from other applications. While OPTICA may be used for the detection and localization of absorptive, scattering, and fluorescent targets, this letter focuses on scattering targets.

The perturbation in the light intensity distribution on the boundaries of the medium, the scattered wave field, due to scattering inhomogeneities is given by[5]

$$\phi_{\mathrm{sca}}(\mathbf{r}_d,\mathbf{r}_s) = -\int d^3r\,\delta D(\mathbf{r})c\nabla_r G(\mathbf{r}_d,\mathbf{r})\cdot\nabla_r G(\mathbf{r},\mathbf{r}_s), \quad (1)$$

in the diffusion approximation (DA). Here, $\mathbf{r}_s$, $\mathbf{r}$, and $\mathbf{r}_d$ are the positions of the source, the inhomogeneity and the detector, respectively, $\delta D = D_{\mathrm{obj}} - D$ is the difference between the diffusion coefficient of the object, D_{obj} and that of the medium, D, c is the speed of light in medium, and $G(\mathbf{r},\mathbf{r}_s)$ and $G(\mathbf{r},\mathbf{r}_d)$ are source-target and target-detector Green's functions, respectively. While the formalism, detailed elsewhere and tested for simulated data,[6] is applicable for different sample sizes and shapes, Green's functions for the slab geometry[7] are used here since rectangular slab samples were used in experiments.

Under the assumption that the scattering inhomogeneities are localized in a few regions within the turbid medium, Eq. (1) may be rewritten as

$$\begin{aligned} -\phi_{\mathrm{sca}}(\mathbf{r}_d,\mathbf{r}_s) = &\sum_{j=1}^{n} g_z(\mathbf{r}_j,\mathbf{r}_d)q_j g_z(\mathbf{r}_j,\mathbf{r}_s) \\ &+ \sum_{j=1}^{n} \rho_{dj}\cos\theta_d g_\perp(\mathbf{r}_j,\mathbf{r}_d)q_j\rho_{sj}\cos\theta_s g_\perp(\mathbf{r}_j,\mathbf{r}_s) \\ &+ \sum_{j=1}^{n} \rho_{dj}\sin\theta_d g_\perp(\mathbf{r}_j,\mathbf{r}_d)q_j\rho_{sj}\sin\theta_s g_\perp(\mathbf{r}_j,\mathbf{r}_s), \end{aligned} \quad (2)$$

where $q_j = \delta D(\mathbf{r}_j)cV_j$ is the strength of the jth scattering inhomogeneity of volume, V_j located at $\mathbf{r}_j$, $\rho_{dj} = [(x_d - x_j)^2 + (y_d - y_j)^2]^{1/2}$, $\rho_{sj} = [(x_s - x_j)^2 + (y_s - y_j)^2]^{1/2}$, and θ_d and θ_s are the polar angles of $\mathbf{r}_d - \mathbf{r}_j$, and $\mathbf{r}_s - \mathbf{r}_j$, respectively, g_z, and $g_\perp$ are the longitudinal and transverse components of the Green's functions, and the summation is over all the inhomogeneities. The contribution to ϕ_{sca} from the jth inhomogeneity consists of three terms. These three terms may be interpreted as contributions from three "virtual sources" $q_j g_z(\mathbf{r}_j,\mathbf{r}_s)$, $q_j\rho_{sj}\cos\theta_s g_\perp(\mathbf{r}_j,\mathbf{r}_s)$, and $q_j\rho_{sj}\sin\theta_s g_\perp(\mathbf{r}_j,\mathbf{r}_s)$ weighted by $g_z(\mathbf{r}_j,\mathbf{r}_d)$, $\rho_{dj}\cos\theta_d g_\perp(\mathbf{r}_j,\mathbf{r}_d)$, and $\rho_{dj}\sin\theta_d g_\perp(\mathbf{r}_j,\mathbf{r}_d)$, respectively. The first virtual source, $q_j g_z(\mathbf{r}_j,\mathbf{r}_s)$ is centrosymmetric, the other two are dumbbell

[a)]Electronic mail: alfano@scisun.sci.ccny.cuny.edu

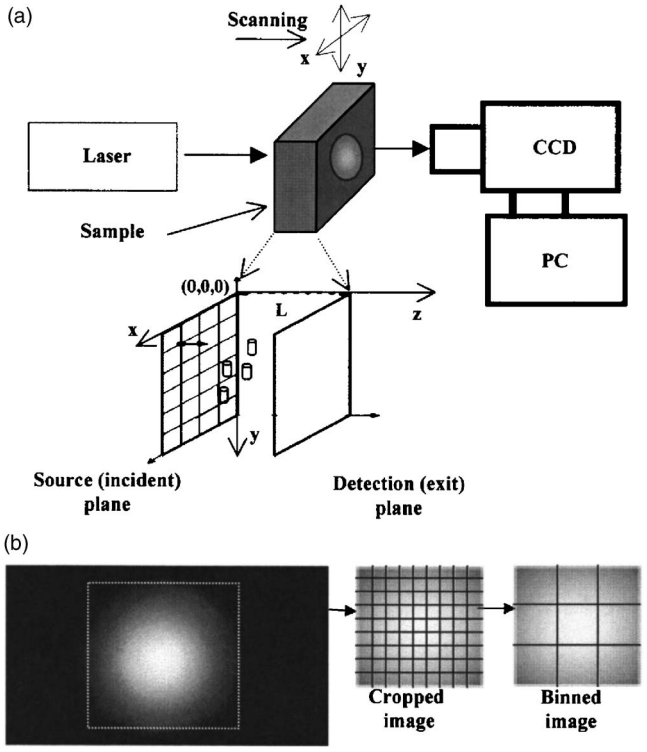

FIG. 1. (a) A schematic diagram of the experimental arrangement. Inset shows a 2D array of horizontal and vertical points in the input plane that are scanned across the laser beam. (b) A typical raw image recorded by the CCD, and how it is cropped and binned for analysis.

shaped and orthogonal to each other. The centrosymmetric virtual source makes the dominant contribution to ϕ_{sca}, compared to the other two. The detected fraction of ϕ_{sca} on the exit plane (also referred to as the detection plane) of the sample is a weighted linear mixture of contributions from $3n$ virtual sources, if there are n scattering targets within the medium. All virtual sources are assumed to be statistically independent.

Independent component analysis of the measured ϕ_{sca} can then retrieve the "virtual sources" and corresponding weighting matrices.[6] The contribution of each target to ϕ_{sca} on the detection plane (and also on the source plane) can be obtained as a two-dimensional (2D) independent intensity distribution (IID). IID due to a target may be looked upon as the light intensity pattern that a source located at the target position would generate on the detection (or source) plane. The 3D location of the target relative to sample boundaries is estimated from fits of these OPTICA generated IID to the model Green's functions.

The experimental arrangement for demonstrating the efficacy of OPTICA is shown schematically in Fig. 1. Continuous-wave 784 nm radiation from a diode laser delivered by a 200-μm-optical fiber was used for illuminating the entrance face (henceforth referred to as the "source plane") of the slab sample. Multiple source illumination was realized in practice by step scanning the slab sample along the horizontal (x) and vertical (y) directions across the laser beam. A camera lens collected the diffusely transmitted light on the opposite face of the slab (henceforth referred to as the "detection plane") sample and projected it onto the sensing element of a cooled charged couple device (CCD) camera. Each illuminated pixel of the 1024×1024 pixels of the CCD camera could be regarded as a detector. For illumination of every scanned point on the source plane, the CCD camera recorded the diffusely transmitted intensity pattern on the detection plane.

Two different samples were used in the experiments reported here. The first sample was a 250 mm $\times$ 250 mm $\times$ 50 mm transparent plastic cell filled with Intralipid-10% suspension in water. The concentration of Intralipid-10% was adjusted to provide a transport length ℓ_t of $\sim$2 mm at 784 nm. A $\sim$9-mm-diameter glass sphere filled with a suspension of 0.707 μm diameter polystyrene spheres in water was the scattering target. The microspheres do not absorb 784 nm light, and their concentration was adjusted to provide a scattering length, ℓ_s of $\sim$0.0188 mm, transport length ℓ_t of $\sim$0.133 mm, and anisotropy factor, $g\sim0.858$. The location of the center of the target was (25 mm, 25 mm, 21 mm) with respect to the front upper left corner of the sample cell [see inset of Fig. 1(a)]. This sample was used to test the predictions of the theoretical formalism.

The second sample was a 166-mm-long, 82-mm-wide, and 55-mm thick scattering slab cast from a suspension of titanium dioxide particles and a near-infrared dye in epoxy resin containing four cylindrical scattering targets.[8] The slab material had an optical transport length of $\sim$1.1 mm, and absorption coefficient of 0.006 mm^{-1}. Each of the four cylinders had a length of 5 mm, a diameter of 5 mm, absorption coefficient equal to that of the slab material, and scattering coefficients 4, 2, 1.5, and 1.1 times higher than that of the slab. The center of each cylinder was located in the plane halfway between the front and back surfaces of the slab, and their known coordinates are presented in Column 3 of Table I. The second sample was used to test the efficacy of OPTICA on a breast-simulating specimen. Sample 1 was scanned in an x-y array of 21×21 grid points with a step size of 2.5 mm across the laser beam, while Sample 2 was scanned in a 20×18 array of same step size.

Figure 1(b) presents a typical 2D raw image of the detection plane recorded by the CCD camera for illumination of a grid point in the source plane. Similar 2D raw images are recorded for every scanned grid point on the source plane. As Fig. 1(b) further shows, each raw image is then cropped to select out the information-rich region, and binned to enhance the signal-to-noise ratio. All the binned images are then added and an average image (henceforth, referred to

TABLE I. Comparison of the known and OPTICA determined positions of the targets in Sample 2.

Target No.	$\mu_{s,\text{target}}/\mu_{s,\text{slab}}$	Known position (x,y,z) mm	Observed position (x,y,z) mm	Error $(\Delta x,\Delta y,\Delta z)$
1	4	(60, 60, 27.5)	(62, 63, 28.1)	(2, 3, 0.6)
2	2	(47, 30, 27.5)	(48, 33, 28.9)	(1, 3, 1.4)
3	1.5	(33, 60, 27.5)	(33, 62, 27.1)	(0, 2, 0.4)
4	1.1	(20, 30, 27.5)	(18, 33, 32.6)	(2, 3, 5.1)

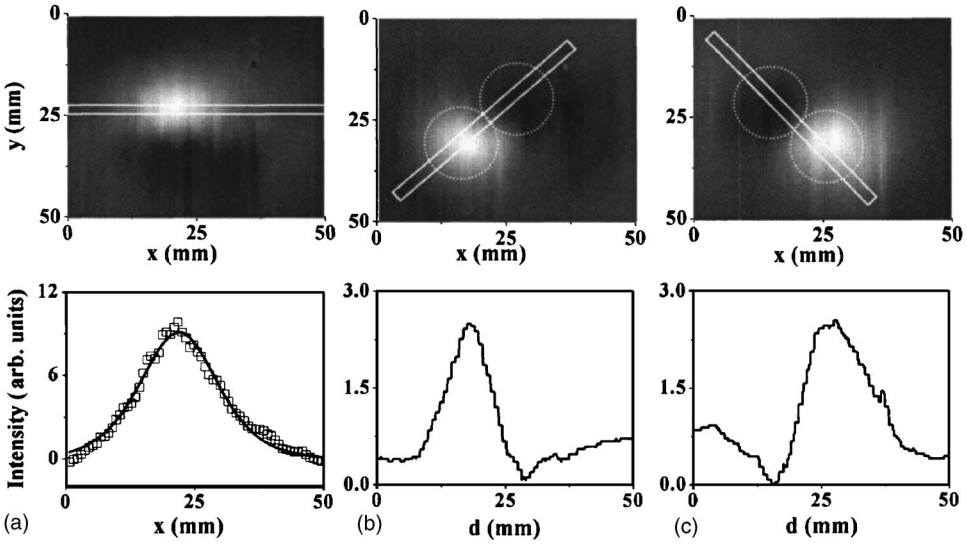

FIG. 2. Independent 2D spatial intensity distributions at the detection plane of the scattering sphere in Sample 1 generated by OPTICA: (a) The centrosymmetric component. (b) and (c) the dumbbell shaped components. The white dotted circles in the images presented in (b) and (c) are provided as guide for the eyes to show the high intensity and low intensity areas of the dumbbell. The white rectangles in the images are the regions that are integrated over to generate the spatial profiles. In the lower frame of (a), the solid line represents a Green's function fit to the experimental data represented by open squares.

as the "reference image") is generated to serve as the background. The difference between the reference image and the mth binned image is proportional to the perturbation in light intensity distribution on the detection plane, $\phi_{\mathrm{sca},m}$ for illumination of the mth grid point. All the $\phi_{\mathrm{sca},m}$'s are then stacked, and used as input for independent component analysis.

OPTICA generated 2D independent intensity distributions (IIDs) at the detection plane for the single scattering target in Sample 1 are presented in the upper frames of Figs. 2(a)–2(c). The corresponding spatial intensity profiles integrated over the areas enclosed by white dashed boxes appear in the lower frames. As predicted by the theoretical formalism, three intensity distributions from three virtual sources corresponding to the single scattering target are observed. The spatial intensity profile of Fig. 2(a) is symmetric about the vertical centerline (centrosymmetric), the profile of Fig. 2(b) has a peak followed by a dip, and that of Fig. 2(c) has a dip followed by a peak, and resemble the predicted dumbbell shape. The location of the target determined from the Green's function fit of the intensity distribution is (23 mm, 25 mm, 22 mm) which agrees well with the known position of (25 mm, 25 mm, 21 mm). The relative peak intensity of the centrosymmetric component is approximately four times larger than that of the dumbbells. For more highly scattering samples and with a decrease in the signal-to-noise ratio, the dumbbell-shaped components get much reduced in intensity, and may not be observable. It should be mentioned that an absorptive target generates only a centrosymmetric IID.

The results of OPTICA measurements on Sample 2 are summarized in Table I, that compares the known locations of all 4 targets with those obtained from this approach. Except for Target No. 4, coordinates of other targets are obtained within 0–3 mm (a standard deviation of ~2 mm) of the respective known positions. The larger error in the estimated location of Target No. 4 may be due to its low contrast and hence higher susceptibility to noise. Overall, the errors in location estimates are smaller than the target dimensions even for a breast-simulating scattering medium.

What is remarkable about the OPTICA approach is that even at this initial stage of development it could detect and locate all four scattering targets, including the weakest target with a scattering coefficient just 1.1 times the background and hence was considered to be "rather unlikely to be found."[8] For highly scattering medium (such as Sample No. 2), only the centrosymmetric virtual sources corresponding to scattering targets could be observed. Additional information, such as measurements at different wavelengths are needed for identification of the target as a scatterer or an absorber. Although the DA was used in this case, OPTICA does not depend on any specific light propagation model, and can be used with other models. This feature makes OPTICA a more general approach applicable for a variety of scattering media where DA may not hold. OPTICA is suited for detection of small inhomogeneities on mm scale, and has the potential for detection and localization of tumors in the breast at early stages of growth.

The research is supported in part by grants from ONR, NASA, and USAMRMC. The authors acknowledge Imtiaz Tanveer for technical help, and Professor Jeremy Hebden of University College London for the loan of Sample 2.

[1] N. Kroman, J. Wohlfahrt, H. T. Mouridsen, and M. Melbye, Int. J. Cancer **105**, 542 (2003).
[2] S. K. Gayen and R. R. Alfano, Opt. Photonics News **7**, 22 (1996).
[3] S. R. Arridge, Inverse Probl. **15**, R41 (1999).
[4] P. Comon, Signal Process. **36**, 287 (1994).
[5] M. Xu, M. Lax, and R. R. Alfano, J. Opt. Soc. Am. A **18**, 1535 (2001).
[6] M. Xu, M. Alrubaiee, S. K. Gayen, and R. R. Alfano, J. Biomed. Opt. **10**, 051705 (2005).
[7] M. Lax, V. Narayanamurti, and R. C. Fulton, in *Laser Optics of Condensed Matter*, edited by J. L. Birman, H. Z. Cummins, and A. A. Kaplyanskii (Plenum, New York, 1987), pp. 229–237.
[8] D. J. Hall, J. C. Hebden, and D. T. Delpy, Appl. Opt. **36**, 7270 (1997).